Journal of Materials Chemistry A

PAPER

View Article Online
View Journal | View Issue

Check for updates

Cite this: J. Mater. Chem. A, 2018, 6, 17633

Efficiently texturing hierarchical superhydrophobic fluoride-free translucent films by AACVD with excellent durability and self-cleaning ability†

Shuhui Li,[ab] Kristopher Page,[b] Sanjayan Sathasivam,[b] Frances Heale,[b] Guanjie He,[b] Yao Lu,[c] Yuekun Lai,*[ad] Guoqiang Chen,[a] Claire J. Carmalt[b] and Ivan P. Parkin*[b]

Translucent and superhydrophobic glass surfaces were fabricated by one-step deposition of a composite from the precursors, polydimethylsiloxane (PDMS) and tetraethyl orthosilicate (TEOS), *via* aerosol-assisted chemical vapour deposition. A raspberry-like hierarchical structure was obtained due to the nanoparticles being decomposed by the TEOS precursor and deposited around the micro-scale particles formed by the hydrolysis of the PDMS precursor. In this work, a translucent and superhydrophobic film was prepared by using optimized parameters (*T*: 290–330 °C, deposition time: 15–30 min) and the resulting water contact angle and sliding angle were >160° and <1°, respectively. It was found that there were 9 bounce cycles when water droplets were dropped onto such surfaces. Superior robustness was observed against tape-peeling, and on exposure to UV light (365 nm, 3.7 mW cm^{-2}, 72 h) and to a large pH range (pH = 1–14, 72 h). The mechanical robustness was also examined and the results demonstrated that the film loses its superhydrophobicity when abraded for 5 meters with coarse sandpaper. The self-cleaning test demonstrated that the superhydrophobic surface could shed various contaminants and aqueous dyes, leaving a clear surface behind. This novel method can be applied to various substrates, including flexible (fabric and copper mesh) and rigid materials (copper block). This can provide a new, rapid and facile route for producing large-scale samples with multifunctional applications.

Received 7th June 2018
Accepted 17th August 2018

DOI: 10.1039/c8ta05402a

rsc.li/materials-a

Open Access Article. Published on 23 August 2018. Downloaded on 3/29/2024 10:03:19 AM.
This article is licensed under a Creative Commons Attribution 3.0 Unported Licence.

1. Introduction

Special wettability surfaces, in particular, superhydrophobic surfaces, have attracted a lot of attention recently because of their applications in a range of fields of materials science and engineering inspired by the "lotus effect" in nature.[1–10] Superhydrophobic surfaces are defined as surfaces with static water contact angles exceeding 150° and sliding angles lower than 10°. As is well known, the superhydrophobic surface depends on the geometrical structure and low surface energy chemical composition.[9,11–19] Superhydrophobic surfaces with such interface behaviour allow water/rain droplets to easily roll off from the substrates and those with high transparency have potential applications in various fields, such as self-cleaning traffic indicators, wind screens, optical devices, self-cleaning windows, solar panels, *etc.* Recently, a lot of researchers have reported the preparation of excellent superhydrophobic surfaces using various methods and have overcome more and more challenges.[20–31] Ji *et al.*[32] reported a facile method to fabricate superhydrophobic glass surfaces *via* a one-step hydrothermal method followed by chemical modification. Martin *et al.*[27] fabricated transparent, wear-resistant, superhydrophobic and superoleophobic surfaces on flat and micropatterned PDMS by coating with hydrophobic SiO_2 nanoparticles and a binder of methylphenyl silicone resin by using a spraying method and subsequent vapour deposition of fluorosilane to achieve superoleophobicity. Zhang *et al.*[28] prepared a novel silica-fibre network structure by soot-assisted CVD technology and then endowed the surface with superhydrophobicity by immersing the sample in a fluorosilane solution. Through calcination at 500 °C with the assistance of O_2 airflow, the soot film was removed and a transparent superhydrophobic film was decorated onto the glass substrate. Though transparent and superhydrophobic glass surfaces have made some progress, the approaches in most cases need strict conditions, sophisticated equipment, or complex fabricating procedures, which limit industrial and practical applications.

[a]National Engineering Laboratory for Modern Silk, College of Textile and Clothing Engineering, Soochow University, Suzhou 215123, China. E-mail: yklai@suda.edu.cn
[b]Department of Chemistry, University College London, London, WC1H 0AJ, UK. E-mail: i.p.parkin@ucl.ac.uk
[c]Department of Mechanical Engineering, University College London, Torrington Place, London, WC1E 7JE, UK
[d]College of Chemical Engineering, Fuzhou University, Fuzhou 350116, China

† Electronic supplementary information (ESI) available. See DOI: 10.1039/c8ta05402a

Open Access Article. Published on 23 August 2018. Downloaded on 3/29/2024 10:03:19 AM.
This article is licensed under a Creative Commons Attribution 3.0 Unported Licence.

Transparent and durable superhydrophobic surfaces have many practical applications and have attracted much attention from researchers.[4,29,33–38] High surface roughness is still the main obstacle to the transparency and durability of super hydrophobic surfaces. A highly rough structured surface can be semi-transparent or opaque due to light scattering, and light scattering can be reduced by decreasing the scale of the surface roughness to a value lower than the wavelength of light.[39] Most of the previous studies on transparent and durable superhydrophobic surfaces were based on carbon derivatives, polymers, and silicon nanoparticles. Huang *et al.*[36] used the sol–gel method to form coatings with silica nanoparticles and silicic acid, optimally achieving superhydrophobicity with an SCA of 160° and an SA of 7° ± 2° and reducing transmittance by less than 5%. Li *et al.*[38] fabricated silica nanoparticle-assembled nanoscale porous structures on glass substrates, showing excellent superhydrophobic properties with a CA of 159.9° ± 2.1°, an SA of 4° ± 0.5° and an average transmittance of 90% in the visible wavelength range. However, though remarkable wettability and transparency were achieved, the durability and robustness of those coatings were inferior due to low adhesion between the nanoparticles and substrate surface.

Aerosol-assisted chemical vapour deposition (AACVD) is an enhanced CVD technology that can operate at ambient pressure, under which the precursor solution is vaporised by transforming it into an aerosol using an ultrasonic humidifier. The precursor solution does not need to be volatile; it must be soluble in a suitable solvent and able to form microdroplets for passing into the heat chamber. Therefore, AACVD technology is an inexpensive, rapid, facile method and it is easy to scale up. Polymers such as PDMS with excellent film-forming ability, hydrophobicity and remarkable optical properties are one of the best materials for designing and preparing durable and superhydrophobic film surfaces. In this paper, a translucent and superhydrophobic PDMS coating was fabricated on glass by introducing roughness using SiO_2 nanoparticles *via* an AACVD method. A raspberry-like hierarchical micro–nano structure can be obtained after combining the hybrid precursors at a suitable temperature. Water droplets dropped on such films could bounce for 9 cycles, almost twice that on a comparable PDMS@glass surface, exhibiting prominent water repellency. The superhydrophobic film on the glass surface retained its anti-wettability after being exposed to UV light for 72 h, tape peeling for 250 cycles and immersion in strong acid/base for 72 h. In addition, this facile and inexpensive method can be applied to various substrates (soft and hard materials).

2. Experimental

2.1 Materials

The Sylgard-184 two-part PDMS elastomer precursor and curing agent were purchased from Univar Specialty Consumables. Tetraethyl orthosilicate (TEOS, 98%) was supplied by Sigma-Aldrich. $NH_3 \cdot H_2O$ (28%) was purchased from VWR international company. Organic solvents, including ethanol and ethyl acetate, were purchased from Fisher Scientific UK and used as supplied. Standard microscope glass slides were purchased from VWR International, Inc. Micro-grained sandpaper (TUFBAK, ADALOX, P1000) was bought from Norton Company. Congo red and methyl blue were supplied by BDH Chemicals Ltd.

2.2 Fabrication of the superhydrophobic film

The Sylgard-184 two-part PDMS elastomer precursor and curing agent were dissolved in 50 mL of ethyl acetate with a weight ratio of 10 : 1 (1.0 g elastomer precursor, 0.1 g curing agent). The mixed solution was marked precursor A and stirred for 20 minutes. Another precursor B was prepared by adding 4.5 mL of TEOS and 4 mL of $NH_3 \cdot H_2O$ into 50 mL of ethanol. Mixture B was magnetically stirred for 1 h before use. Subsequently the reaction precursor was formed by mixing precursors A and B in various volume ratios (1 : 0, 1 : 1, 3 : 1, 6 : 1, 12 : 1, and 24 : 1). The volume of the mixed precursor for the AACVD reaction was 25 mL. Film deposition was carried out in a cold-walled horizontal-bed CVD reactor. The reactor was assembled in a top-down heating configuration, with the carbon heating block positioned above a plate (145 mm × 45 mm × 4 mm) supporting the substrates (glass, silicon, aluminium, stainless steel or copper) 5 mm below and parallel to the carbon block. The complete assembly was enclosed within a quartz tube. Upon reaching the set reactor temperature (200 °C, 250 °C, 290 °C, 310 °C, 330 °C, 350 °C and 400 °C), a PIFCO ultrasonic humidifier (power = 25 W, frequency = 40 kHz) was used to form a precursor aerosol, which was transported to the heated substrate using nitrogen carrier gas (1 L min^{-1}). Depositions were carried out for various durations (5 min, 10 min, 15 min, 20 min, 25 min and 30 min), and then the PDMS/TEOS coated substrates were cooled under nitrogen and then handled in air.

2.3 Characterization

The surface morphologies of the as-prepared samples were studied with a JEOL JSM-6301F field emission scanning electron microscope (SEM). The samples were vacuum sputtered with a thin layer of gold to improve the surface electrical conductivity prior to observation. The as-prepared glass films were cut into small pieces and placed on the holder perpendicularly by using carbon double side tape; subsequently a thin layer of gold was sputtered for visualizing the interface. The average thickness of the as-prepared films was statistically analysed with Image J software by counting 20 data points at different positions. UV-vis spectra were recorded using a Shimadzu UV-2600 spectrometer single beam instrument over a range of 200–1000 nm wavelengths. ATR-FTIR measurements were taken over a range of 400–4000 cm^{-1} using a Platinum ATR (BRUKER) equipped with a single reflection diamond attachment. X-ray photoelectron spectroscopy (XPS) was carried out using a Thermo Scientific K-α photoelectron spectrometer; the C 1s peak at 284.6 eV was used as a reference. Water contact angle (CA) measurements were performed by using an FTA-1000 drop shape instrument (First Ten Angstroms Inc.) with a 7 μL water droplet and the CA values were estimated by the measurement software according to the fitting method using the Young–Laplace equation. Sliding angle (SA) measurements were performed

 This journal is © The Royal Society of Chemistry 2018

Open Access Article. Published on 23 August 2018. Downloaded on 3/29/2024 10:03:19 AM.
This article is licensed under a Creative Commons Attribution 3.0 Unported Licence.

using the tilted drop method, with a water droplet size of 15 μL. At least 6 different positions on each sample were tested. A high-speed camera (fps1000HD, The Slow Motion Camera Company, UK) was used to record the bounce dynamics of water droplets on the as-prepared superhydrophobic surfaces at a frame rate of 1000 frames per second. The distance between the pipette tip and the sample surface was fixed at 2 cm and the volume of dispensed water was 8 μL. Individual frames were collected from the camera as digital negative (.DNG) files and processed using DaVinci Resolve 14 (Blackmagic Design Pte. Ltd.) and Adobe Bridge CS5.1 with Camera Raw (Adobe Inc.).

2.4 The mechanical robustness property

The mechanical robustness of the as-prepared PDMS/TEOS@glass surface was demonstrated by using micro-grained sandpaper (TUFBAK, ADALOX, P1000) which was bought from Norton Company as an abrasive material. A 26 × 26 mm sample was placed onto the sandpaper with the PDMS/TEOS@glass film to be tested facing the sandpaper, and then a 100 g weight was put in the middle of the sample. The sample was moved 20 cm across the sandpaper by an external force parallel to the substrate. The sample was rotated 90° clockwise after each abrasion to make sure the sample was abraded in all four directions. The water droplet contact angles (CA), sliding angles (SA) and SEM images of the samples were taken after abrasion tests.

2.5 Durability testing

To investigate the durability of the as-prepared superhydrophobic PDMS/TEOS@glass film, various experiments were carried out including the tape peeling test, UV resistance test and anti-corrosion test. The resultant changes in CAs and SAs for each test were recorded to demonstrate the retention of superhydrophobic behaviour. The tape peeling test was conducted by using a common double-sided tape to investigate the adhesion between superhydrophobic PDMS/TEOS films and the glass substrates, and the CAs and SAs were measured after every 20 cycles. In order to investigate the UV exposure performance, the samples were exposed to UV light (365 nm, 3.7 mW cm^{-2}) for 72 h at room temperature, and the CAs and SAs were measured after every 24 hours. The anti-corrosion test was performed by immersing the superhydrophobic surfaces in either hydrochloric acid solution or sodium hydroxide solution (either 1 or 14) for 72 h. After that, the samples soaked in different acid/base solutions were selected for water droplet bouncing tests.

2.6 Self-cleaning ability

To demonstrate the self-cleaning property of the as-prepared superhydrophobic films, coal ashes and various dye powders including Congo red and methyl blue were chosen as model dust/contaminants to be dispersed on the film surface. The superhydrophobic PDMS/TEOS glass was leant against a Petri dish with a determined tilt angle. Then, water droplets were continuously dropped onto the contaminated surfaces and the powders were picked up, dissolved and carried away by the water droplets, finally leaving behind a very clear surface. This phenomenon demonstrated that the as-prepared film possessed low surface energy and excellent superhydrophobic properties.

3. Results and discussion

There are several fundamental steps in the formation of desired materials in any AACVD reaction process. When the precursors are atomised by using an ultrasonic humidifier the precursor mists will be carried to the reactor by nitrogen gas. As shown in Fig. 1a, once the precursor mist passes through the heated substrate, the solvent will evaporate and the precursors can react with each other to form the desired materials. Meanwhile, waste products are carried away to the exhaust. With time, more and more precursors nucleate and aggregate together and finally result in the formation of a film. In general, there are five steps during the AACVD process:[40] (I) the gas phase reaction of the different mixed precursors, (II) the precursors pass through the boundary layer to be adsorbed onto the substrate surface, (III) the precursors nucleate and react at high temperature, (IV) emission of waste products, and (V) more molecules of the precursors are adsorbed resulting in the film growth. The mechanism shows the formation process of hierarchical morphology on the as-prepared film. The surface morphology of the as-prepared PDMS/TEOS@glass (330 °C, 30 min) is shown in Fig. 1b. It is very obvious that micro-sized spherical particles were surrounded by a number of nano-sized particles with a diameter of approximately 100 nm. Such a "raspberry-like" hierarchical structure can increase the surface roughness and be very beneficial for superhydrophobicity, leading to a larger static water contact angle of around 166.1°. However, the contact angle for a water droplet on the blank glass was about 25.7°, indicating that the bare glass was intrinsically hydrophilic as expected (Fig. S1†).

A high-speed camera was used to capture the bouncing behaviour of water droplets on the superhydrophobic surface at room temperature. As shown in Fig. 1c, an 8 μL droplet of water

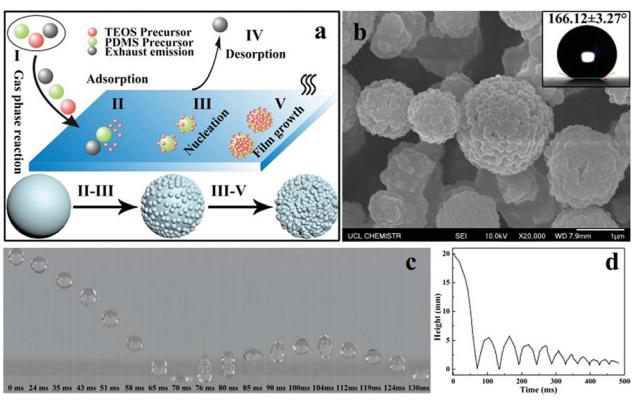


Fig. 1 (a) The formation mechanism of film growth by the AACVD process. (b) The SEM image of the as-prepared superhydrophobic PDMS/TEOS@glass (330 °C, 30 min), inset is the corresponding static water contact angle. (c) Water bouncing test (8 μL) on the as-prepared superhydrophobic surface and changes of the distance between the water droplet and substrate surface during the bouncing test (d).

Open Access Article. Published on 23 August 2018. Downloaded on 3/29/2024 10:03:19 AM.
This article is licensed under a Creative Commons Attribution 3.0 Unported Licence.

was released from a height of 2 cm above the superhydrophobic film surface and a high-speed camera was used to capture the dynamic bouncing behaviour of the water droplet on the superhydrophobic PDMS/TEOS@glass surface. The water droplet began to impact the superhydrophobic surface for the first time at a speed of 0.63 m s^{-1} when $t = 63$ ms and then the deformation of the water shape could be observed. The water droplet moved upwards until its velocity reduced to 0 m s^{-1} where the height of the water droplet was 5.5 mm ($t = 104$ ms). The curve of the height of the water droplet at different times indicated that there were 9 bounce cycles, which was attributed to the low adhesive force between the water and superhydrophobic film. The whole movement of the water droplet on the superhydrophobic film can be seen in Video S1.† However, water droplet impact on the blank glass showed no bouncing behaviour, which is due to the high hydrophilicity of the glass surface (Video S2†). The number of bounces of a water droplet dropped onto a superhydrophobic surface depends on the surface microstructure, surface tension and static contact angle. Crick *et al.*[24,41] investigated the relationship of the water bouncing with the water contact angle (0–180°) and surface microstructure with either rounded, sharp or very sharp (needle-like) structures. They found that water bouncing only occurred on surfaces with a water contact angle over 151° for a rounded surface microstructure. Recently, 14 bounces were achieved on a surface with a contact angle of 175° from a height of 20 mm by using an 8 μL water droplet. In addition, 7 bounces were found on the superhydrophobic surface agglomerated with the Sylgard 184 elastomer rounded structure (when water contact angle $\theta = 165°$). In our work, though excellent anti-wettability can be obtained for the PDMS@glass sample ($\theta = 155°$), fewer bounce motions (about 4 bounces) were recorded in comparison with the PDMS/TEOS@glass sample, indicating that the hierarchical structure had a significant effect on improving superhydrophobicity (Video S3†).

A rough structure plays an important role in the construction of superhydrophobic surfaces. For the sake of constructing a suitable micro/nano hierarchical structure, the volume ratios of precursor PDMS and precursor TEOS were adjusted to obtain different hybrid precursor solutions. The results, shown in Fig. S2,† exhibited various surface morphologies; when the volume ratios were 1 : 1 and 3 : 1, nanoparticles surrounding microparticles were observed. On further increasing the volume ratio, the number of nanoparticles can be observed to reduce. The results of wettability on such surfaces indicated that both the static water contact angle and dynamic sliding angle can be optimised when the volume ratios were 1 : 1 and 3 : 1 (Fig. S3†). However, the film prepared with a volume ratio of 1 : 1 was easily removed by a finger wipe. Interestingly, by mixing different volumes of the precursor TEOS, the sliding angle of the as-prepared film surface reduced to almost 8° in comparison with that prepared with a non-mixed precursor, which further indicated that the micro/nano hierarchical structure has a significant effect on superhydrophobicity. Therefore, the volume ratio was recognized as the optimum parameter for further research. In order to investigate the formation mechanism of the compound precursors on the glass substrate by AACVD, we have also prepared various superhydrophobic films deposited at different reaction temperatures for 30 min (200 °C, 250 °C, 290 °C, 330 °C, 350 °C, and 400 °C). Fig. 2 shows the SEM images of a single PDMS precursor at a fixed temperature (330 °C) and hybrid precursors at various temperatures. The results indicated that the reaction temperature had a significant influence on the surface morphology. When just using the PDMS polymer as a precursor, we can observe numerous micron-sized particles ranging from 0.5 μm to 2 μm deposited on the glass surface. These regular spherical particles coalesced into irregular and bigger particles (Fig. 2a). Once TEOS solution was added into the PDMS precursor, the surface morphology of the film changed. Nanoparticles with a diameter of about 100 nm could be found surrounding the microparticles. The micro-sized particles were made of the PDMS polymer and the nano-size particles were considered as silicon dioxide, which was generated from the hydrolysis of TEOS. In addition, the size of the particles did not change significantly but the number increased with temperature (200–290 °C). When the temperature was elevated to 350 °C, the size of the microparticles and the number of nanoparticles deposited on the glass substrate decreased compared with that prepared at 290 °C. Upon increasing the temperature to 400 °C, the particles were observed to become further smaller and again fewer in number, which is likely due to the precursor being mostly cured and pyrolysed into smaller particles at higher temperatures prior to deposition. However, at these elevated temperatures, the superhydrophobicity and robustness were poor; the film can be wiped away just by using a finger. As a result, the raspberry-like hierarchical micro/nano particles can be best fabricated at 290–330 °C.

Fig. 3(a) shows the FT-IR spectra of the TEOS precursor, PDMS@glass film and PDMS/TEOS@glass film from 4000 to 400 cm^{-1}. This provides evidence for the hydrolysis of TEOS and the copolymerization between PDMS and the silica matrix. Three obvious peaks were observed at 1072 cm^{-1}, 945 cm^{-1}, and 800 cm^{-1} and assigned to the Si–O stretching, Si–OH band and Si–O–Si symmetric stretching vibration of the TEOS precursor, respectively, indicating that hydrolysis and polymerization of TEOS occurred.[42,43] The bands observed at

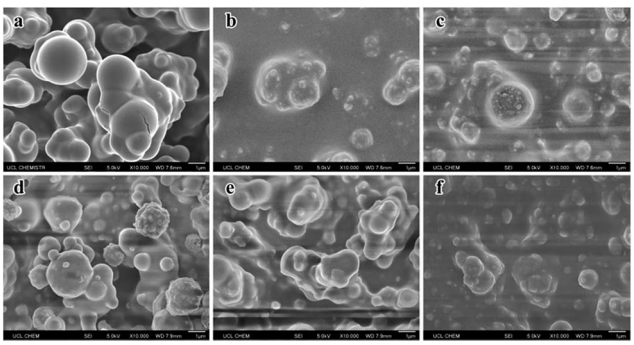


Fig. 2 The surface morphologies of PDMS@glass (a) and the as-prepared PDMS/TEOS@glass substrate at various reaction temperatures with deposition for 30 min: 200 °C (b), 250 °C (c), 290 °C (d), 350 °C (e), and 400 °C (f).

 This journal is © The Royal Society of Chemistry 2018

Open Access Article. Published on 23 August 2018. Downloaded on 3/29/2024 10:03:19 AM.
This article is licensed under a Creative Commons Attribution 3.0 Unported Licence.

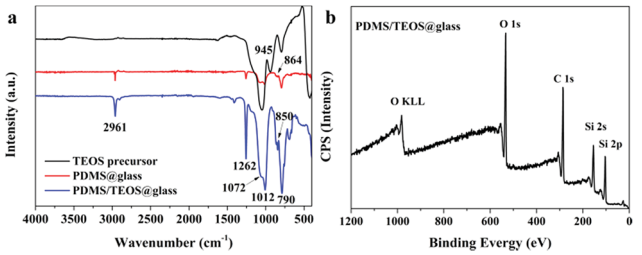


Fig. 3 (a) FTIR spectra of the as-prepared TEOS precursor, PDMS@glass film, and PDMS/TEOS@glass film and the XPS spectrum (b) of the as-prepared superhydrophobic film surface.

2961 cm^{-1} and 1262 cm^{-1} were attributed to the asymmetric CH_3 stretching and CH_3 deformation in Si–CH_3 of PDMS.[44] The peaks at 864 cm^{-1} and 790 cm^{-1} were determined as the Si–$(CH_3)_2$ stretching vibration of PDMS. The peaks with strong intensity at 1012 cm^{-1} were assigned to the asymmetric stretching of Si–O–Si. The bands around 430–780 cm^{-1} can be attributed to the rocking transverse and symmetric stretching of Si–O bonds.[45,46] The band observed at 850 cm^{-1} is directly assigned to the copolymerization of PDMS and TEOS.[47–49] The surface chemical composition of the PDMS/TEOS@glass surface was further confirmed by XPS. The result shown in Fig. 3b indicates that such a superhydrophobic surface was composed of carbon, oxygen and silicon elements.

In order to investigate the relationship between the reaction time and the transparency and superhydrophobicity, the precursor was deposited at a fixed temperature (330 °C) for 5 min, 15 min, 20 min, and 30 min. Fig. 4 shows cross-sectional, top-down SEM images, contact angles and photographs showing the visible transparency for the PDMS/TEOS@glass films with different reaction durations. The sample deposited for 5 min as shown in Fig. 4(a1) had the thinnest film (approx. 1.5 μm) which exhibited the best transparency, but the lowest water contact angle of 119.7 ± 3.0°. The roughness values R_a and R_q for the sample deposited after 5 min were 68.2 nm and 87.8 nm from the AFM 3D photographs, while roughness values R_a and R_q for the blank glass were 0.515 nm and 0.655 nm, respectively (Fig. S4†). The film deposited for 15 min had a thicker and rougher texture (thickness: 2.58 ± 0.69 μm) than the sample prepared for 5 min (thickness: 1.81 ± 0.55 μm). However, the static water contact angle dramatically increased to 156.9 ± 0.8° and more haze can be found on this film. Deposition for another 5 minutes showed that a slight increase of around 2° in the water contact angle could be obtained and the surface morphology was rougher (thickness: 4.19 ± 1.21 μm), demonstrating that the surface roughness plays a great role in improving superhydrophobicity. However, the transparency decreased a little. At a reaction time of 30 minutes, the as-prepared glass was hazier since it was the thickest and densest film (thickness: 4.28 ± 0.52 μm). This film gives excellent superhydrophobic properties with a high water contact angle (>162°) and low sliding angle (~0°).

It is well known that the surface wettability is dependent on the surface morphology, structure and surface chemistry. In this work, we demonstrate a very versatile method utilising PDMS as the main precursor and combining it with nanoparticles generated from the hydrolysis of TEOS to generate a superhydrophobic film by a one-step AACVD method. We have done a batch of experiments in order to investigate the relationship between the wettability (static contact angle and dynamic sliding angle) of the film surface and the reaction conditions (temperature, time and precursor volume ratio). As shown in Fig. 5a, the WCAs of the as-prepared PDMS/TEOS@glass films with a deposition time of 30 min kept a stable level around 160° except the sample prepared at 200 °C, which exhibited hydrophobicity with the CA approximately 120°. This is because most of the precursor existed in the form of an aerosol and discharged to the exhaust under N_2 gas at lower temperature. The temperature was insufficient to enable precursor decomposition into particles and their deposition onto the glass surface. If the temperature of deposition is

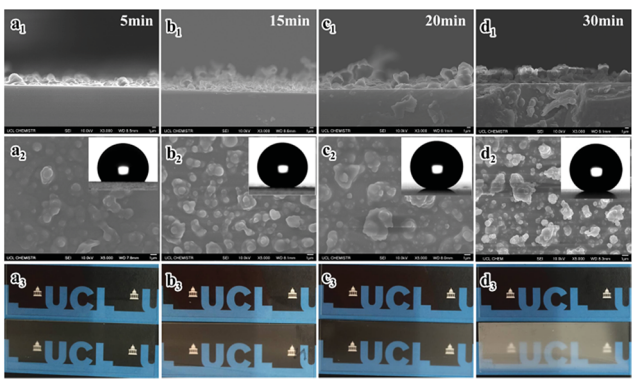


Fig. 4 The cross-sectional (a_1–d_1), top-down SEM images and contact angles (a_2–d_2) of the PDMS/TEOS@glass samples fabricated at a fixed temperature of 330 °C with different deposition times (5 min, 15 min, 20 min, and 30 min); (a_3–d_3) are the corresponding optical images showing visible transparency.

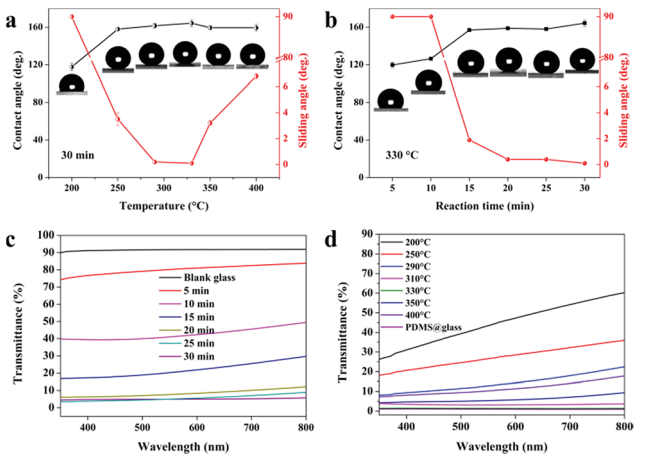


Fig. 5 The relationship of contact angles and sliding angles with reaction temperature (a) and reaction time (b) and the transparency on blank glass and the as-prepared PDMS/TEOS@glass surfaces at 330 °C with different deposition times (c) and deposition for 30 min at various deposition temperatures (d).

Open Access Article. Published on 23 August 2018. Downloaded on 3/29/2024 10:03:19 AM.
This article is licensed under a Creative Commons Attribution 3.0 Unported Licence.

increased to above 250 °C, the WCAs dramatically increased to around 160° and the dynamic sliding angle decreased to below 10°. When the reaction temperature was above 330 °C, the sliding angle appeared to increase slightly which is attributed to the changes in surface morphology as discussed previously.

The relationship between surface wettability and roughness can be confirmed by the following Cassie–Baxter equation:

$$\cos\theta_\gamma = f(1 + \cos\theta) - 1 \quad (1)$$

here, θ_γ and θ are contact angles for water droplets on the rough and untextured surfaces, respectively and f is the fraction of liquid on the composite surface. Since the contact angle θ on an untextured surface is constant, a lower liquid–solid surface ratio f would lead to a higher contact angle θ_γ of the superhydrophobic surface. The water contact angle on the flat PDMS glass surface was 108.8° and the f values calculated for the PDMS/TEOS@glass surfaces were 0.791, 0.108, 0.076, 0.055, 0.093, and 0.094 at 200 °C, 250 °C, 290 °C, 330 °C, 350 °C, and 400 °C, respectively.

In addition, we have also examined the changes in various as-prepared samples at 330 °C with different reaction times (5 min, 10 min, 15 min, 20 min, 25 min, and 30 min). The results in Fig. 5b showed that if the reaction time was below 10 minutes, water droplets could not roll away even when tilting the sample to 90° indicating Wenzel behaviour. On increasing the reaction time to 15 minutes, the superhydrophobicity was significantly improved and water droplets could roll away rapidly when tilted by no more than 2°, indicating that an excellent superhydrophobic film can be obtained in a very short reaction time (15 min). This is due to changes in surface morphology and thickness; when the reaction proceeded for 10 min, a relatively thin layer was formed and the particles were prone to grow parallel to the substrate due to the amount of interspaces used within the reaction time. This resulted in some parts being superhydrophilic/hydrophilic. When a water droplet was dropped onto such a surface, a higher adhesive force was observed between the water droplets and the substrate. This resulted in a "Wenzel state" with water pinning onto such a film. When the film was deposited for a further 5 min, the cavities were filled in and particles aggregated in the vertical direction. This could capture more air and keep the water droplet out of contact with the substrate, thus demonstrating a "Cassie state" with water rolling away from the surface. Similarly, the f values were calculated for the PDMS/TEOS@glass films to be 0.744, 0.600, 0.118, 0.100, 0.107, and 0.055 with different deposition times (5 min, 10 min, 15 min, 20 min, 25 min and 30 min, respectively) at 330 °C according to eqn (1).

The visible transparency of the as-prepared films was measured. Blank glass had about 92% visible transmittance. The transmittance curves are given in Fig. 5c and d to demonstrate how the transparency varies with the deposition time and deposition temperature over a wavelength range from 350 nm to 800 nm. The sample deposited for 5 min gave the highest transparency (around 80%) and when the deposition time increased to 10 min, the transparency reduced to 40–50%. However, a dramatic increase in superhydrophobicity occurred when deposited for 15 min but transparency decreased to < 30%. With deposition times greater than 20 min, a higher water contact angle and lower sliding angle could be obtained, but at the expense of lower transparency (<10%). The transparency of the as-prepared films at various temperatures has also been investigated. In general, superhydrophobicity and transparency are in competition and depend on the thickness of the film and the degree of surface morphology. A higher transparency (<50%) was found at lower temperature (200 °C) and the transparency decreased as the temperature increased. This is due to a more textured and rough morphology on the as-prepared superhydrophobic glass surface at higher temperatures. The results of the transparency tests are in agreement with those obtained from SEM, CA and SA. Moreover, the PDMS@glass film looks white and hazy, which illustrates that the single PDMS polymer is not a good choice for preparing translucent superhydrophobic glass.

Environmental stability is a very significant factor for practical applications. Here, we investigated the stability of the films when exposed to UV light, tape peeling and immersion in a corrosive solution (acid/base). As shown in Fig. 6a, when exposed to UV light (365 nm, 3.7 mW cm^{-2}) for 72 h, the CAs and SAs of the as-prepared superhydrophobic samples (deposition temperature: 310 °C, deposition time: 30 min) were recorded every 12 h. The results showed no obvious changes in the wettability and the resulting sample exhibited excellent UV stability with the water contact angle > 162° and sliding angle < 0.5° during the whole irradiation process. This is due to the superior UV stability of PDMS and SiO_2, which cannot be easily degraded by UV light. Furthermore, to investigate the adhesion between the superhydrophobic film and glass substrate, we conducted a series of tape peeling experiments by using a commercial tape repeatedly stuck to the film surface and removed from its surface. The CAs and SAs were measured after

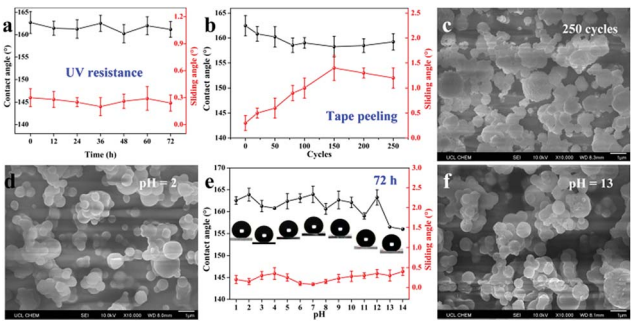


Fig. 6 The contact angles and sliding angles of the as-prepared superhydrophobic PDMS/TEOS@glass surface (deposition temperature: 310 °C, deposition time: 30 min) after UV exposure (365 nm, 3.7 mW cm^{-2}) for various times (a) and tape peeling for different cycles (b). The SEM surface morphology after tape peeling for 250 cycles (c); the changes on CAs and SAs when the superhydrophobic film is immersed in hydrochloric acid solution and sodium hydroxide solution (pH = 1–14) for 72 h (e); insets in (e) are optical images for static water contact angles; the SEM images in (d and f) are for samples immersed in HCl solution (pH = 2) and NaOH solution (pH = 13) for 72 h.

This journal is © The Royal Society of Chemistry 2018

Open Access Article. Published on 23 August 2018. Downloaded on 3/29/2024 10:03:19 AM.
This article is licensed under a Creative Commons Attribution 3.0 Unported Licence.

20, 50, 80, 100, 150, 200, and 250 cycles (Fig. 6b). A slight decrease in the static water contact angle can be observed and the sliding angle increases to around 1° with the first 150 cycles of tape peeling. After that, the sliding angle was maintained at 1.3° for 250 cycles of tape peeling. In addition, the SEM image as shown in Fig. 6c demonstrated that the surface morphology of the film was not destroyed, displaying a robust and firm film.

For corrosion testing of the as-prepared superhydrophobic glass (deposition temperature: 310 °C, deposition time: 30 min), each piece of glass sample was immersed in hydrochloric acid solution and sodium hydroxide solution with a wide pH range from 1 to 14 for 72 h. There was little effect on both CAs and SAs for the wettability of superhydrophobic glass (Fig. 6e). The CAs were still >160° but showed a slight decrease after soaking at pH = 13 or 14 but the SAs were all lower than 0.5° after soaking in both hydrochloric acid solution and sodium hydroxide solution. The surface morphologies after immersing at pH = 2 and pH = 13 conditions were also observed, as shown in Fig. 6d and f. As can be seen from SEM images, there are no obvious changes to the surface resulting from exposure to corrosive solutions since the superhydrophobicity of the film can prevent the corrosive solution from coming into contact with the film surface directly. The samples after soaking in a strong acid/base solution (pH = 2, 7, 13) for 72 h still have excellent bouncing behaviour (Video S4–S6†). Moreover, we have also investigated organic solvent-resistance by soaking the as-prepared superhydrophobic films (deposition temperature: 310 °C, deposition time: 30 min) in organic solutions with different polarities for 3 days; the results demonstrated stable superhydrophobicity (Fig. S5†). The mechanical robustness property is very important in many applications. We conducted the mechanical robustness test by using sand paper and the film was abraded for 1 meter and 5 meters. The results in Fig. S6(a)† showed minor scratches in the SEM morphology but the film was still able to repel water over the defect, having a water contact angle of 155.3° and a sliding angle around 1° after 1 m of abrasion. However, once abraded for 5 m distance, a very clear rectangular shaped scratch appeared which was caused by changing the direction of movement clockwise every 20 cm. Consequently, the water contact angle decreases due to the destruction of the surface structure and a 137.0° contact angle was obtained over the defect. A larger sliding angle was needed for the water droplet to roll away suggesting that the damage to the surface had increased the pinning of droplets placed on the defects. Generally speaking, the mechanical robustness is dependent on the thickness and surface structure of the film. The thicker the film, the lower its transparency but the higher its robustness. Moreover, Zhuang *et al.*[50] reported a dynamic temperature method to prepare a layered film with horizontal strata of varying robustness, which can improve the mechanical robustness demonstrably. However, the transparency of the film would decrease rapidly.

The self-cleaning performances of blank glass and the as-prepared PDMS/TEOS@glass (deposition temperature: 250 °C, deposition time: 30 min) were demonstrated by using Congo red dye as a model contaminant. As shown in Fig. 7a, a sparse layer of dye powder was deposited on the two different

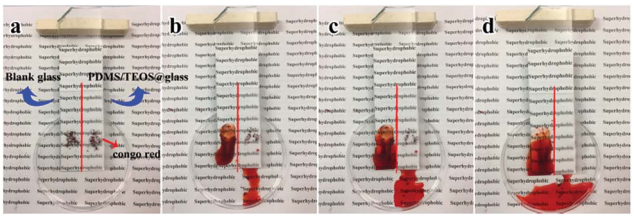


Fig. 7 The self-cleaning process of the blank glass (left) and as-prepared PDMS/TEOS@glass film surface (deposition temperature: 250 °C, deposition time: 30 min) (right), Congo red dye regarded as the model contaminant.

wettability surfaces (left: blank glass, right: superhydrophobic glass) which were put together side by side at an inclination. Subsequently the surface was cleaned directly with a jet of water from a micropipette. During the self-cleaning process, it can be seen that the contaminant can be immediately picked up and dissolved by water droplets for both the hydrophilic blank glass and superhydrophobic glass. However, water droplets would aggregate together and form a puddle of dye liquid on the glass substrate. For the superhydrophobic film, the Congo red dye powder can be quickly picked up, dissolved and carried away from the glass surface, leaving behind a clear surface. In addition to the self-cleaning ability, the optical image for the as-prepared superhydrophobic film was observed to be translucent compared to that of blank glass. The results indicated that a superhydrophobic coating is more beneficial to maintain a tidy and clean surface. For visible effect, we used glitter as the contaminant and took videos of the blank glass and PDMS/TEOS@glass (Videos S7 and S8†).

This facile route can also be applied to various substrates including flexible materials such as cotton and copper mesh and hard materials such as copper blocks at different deposition temperatures for 30 min. Fig. 8 shows the SEM morphologies and water contact images for different substrates. The particle size ranges from 1 μm to 3 μm and the particles were observed to be distributed on the substrate surface evenly. The optical images of dyed water droplets on the substrate indicated that superhydrophobicity has been successfully obtained. As mentioned above, such superhydrophobic films possess superior superhydrophobicity, excellent optical performance and environmental stability. In our previous research, we have investigated the fabrication of a micro/nanostructure "flower-like" TiO_2@cotton fabric surface with special wettability by a hydrothermal or waterbath method.[51,52] Superior properties have been achieved in previous studies compared with this study, but here we adopted a highly efficient one-step synthesis of a superhydrophobic film by AACVD, which is easier to perform, is time-saving (about 30 min), expanding the types of precursors and involves low cost chemical reagents. Moreover, this facile technology can be applied to various substrates, which would expand the range of practical applications, for example for building curtain walls, glasses/bathroom glasses or automotive products such as window glass. Optical transparency is a very special and important property and the preparation of transparent superhydrophobic surface is beneficial to

Open Access Article. Published on 23 August 2018. Downloaded on 3/29/2024 10:03:19 AM.
This article is licensed under a Creative Commons Attribution 3.0 Unported Licence.

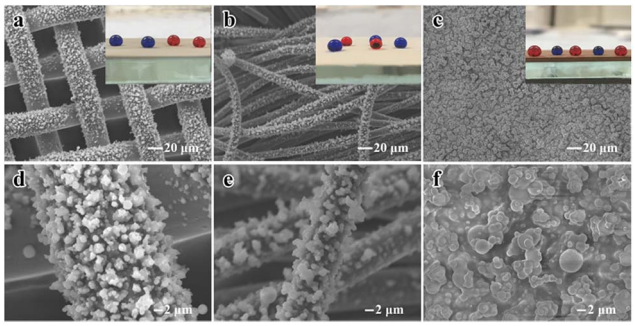


Fig. 8 The SEM morphologies of low and high magnification for various substrates after deposition for 30 min: copper mesh (deposition temperature: 310 °C) (a and d) cotton (deposition temperature: 280 °C) (b and e) and copper block (deposition temperature: 330 °C) (c and f); insets in (a–c) are the optical images of dyed water droplets on each surface.

human life. For engineering materials, the superhydrophobic behaviour of water or other corrosive droplets can greatly enhance their corrosion resistance and prolong their service life in harsh corrosive environments. It is very important and has profound significance in preparing engineering alloy materials with the corrosion resistance of superhydrophobic ability especially for the marine shipbuilding industry.

4. Conclusions

Translucent and superhydrophobic films can be fabricated on a wide range of substrates by a very facile and repeatable route utilising an aerosol-assisted chemical vapour deposition technique. The surface morphology of the as-prepared film was characterized by SEM and microparticles with diameters ranging from 1–2 μm were surrounded by a number of nanoparticles and exhibited excellent water repellent properties with CAs > 160° and SAs < 1°. Water droplets impacting such superhydrophobic films can maintain 9 bounce cycles. Meanwhile, the as-prepared superhydrophobic film also showed excellent environmental stability when exposed to UV light, tape-peeling and corrosive solutions (pH = 1 to 14). The robustness results indicated that after a rigorous abrasion test with sand paper moved over a 1 m distance, the film retains good repellency. This easy and versatile method for deposition of a polymer precursor is suitable for fast and large-scale preparation of robust superhydrophobic films on various substrates across a wide range of temperatures. AACVD is a simple and versatile method as a thin film deposition technique and can provide a potential route by using a single solution to fabricate multi-functionality films. This technology is expected to be able to be applied in many fields such as building curtain walls, self-cleaning glasses (bathroom glass and window glass), engineering materials, marine shipbuilding industry, *etc.*

Conflicts of interest

There are no conflicts to declare.

Acknowledgements

The authors acknowledge the National Natural Science Foundation of China (21501127) and the Priority Academic Program Development of Jiangsu Higher Education Institutions (PAPD) for financial support. S. H. L. is thankful for the funding from the China Scholarship Council (CSC). C. J. C., I. P. P., K. P. and F. L. H. acknowledge AzkoNobel, InnovateUK (192541) and EPSRC for a studentship (FLH) through the Molecular Modelling and Materials Science Doctoral Training Centre (EP/L015862/1) and funding (EP/N510051).

Notes and references

1 S. T. Wang, K. S. Liu, X. Yao and L. Jiang, *Chem. Rev.*, 2015, **115**, 8230–8293.
2 C. Neinhuis and W. Barthlott, *Ann. Bot.*, 1997, **79**, 667–677.
3 A. Nakajima, A. Fujishima, K. Hashimoto and T. Watanabe, *Adv. Mater.*, 1999, **11**, 1365–1368.
4 X. Deng, L. Mammen, H. J. Butt and D. Vollmer, *Science*, 2012, **335**, 67–70.
5 H. Bellanger, T. Darmanin, E. T. de Givenchy and F. Guittard, *Chem. Rev.*, 2014, **114**, 2694–2716.
6 K. S. Liu and L. Jiang, *Nano Today*, 2011, **6**, 155–175.
7 M. Y. Cao, K. Li, Z. C. Dong, C. M. Yu, S. Yang, C. Song, K. S. Liu and L. Jiang, *Adv. Funct. Mater.*, 2015, **25**, 4114–4119.
8 S. H. Li, J. Y. Huang, Z. Chen, G. Q. Chen and Y. K. Lai, *J. Mater. Chem. A*, 2017, **5**, 31–55.
9 H. Zhou, H. X. Wang, H. T. Niu, A. Gestos, X. G. Wang and T. Lin, *Adv. Mater.*, 2012, **24**, 2409–2412.
10 H. Zhou, H. X. Wang, H. T. Niu, A. Gestos and T. Lin, *Adv. Funct. Mater.*, 2013, **23**, 1664–1670.
11 L. W. Chen, Z. G. Guo and W. M. Liu, *J. Mater. Chem. A*, 2017, **5**, 14480–14507.
12 J. Yong, F. Chen, Q. Yang, G. Du, C. Shan, H. Bian, U. Farooq and X. Hou, *J. Mater. Chem. A*, 2015, **3**, 9379–9384.
13 C. Y. Cao, M. Z. Ge, J. Y. Huang, S. H. Li, S. Deng, S. N. Zhang, Z. Chen, K. Q. Zhang, S. S. Al-Deyab and Y. K. Lai, *J. Mater. Chem. A*, 2016, **4**, 12179–12187.
14 H. Liu, Y. D. Wang, J. Y. Huang, Z. Chen, G. Q. Chen and Y. K. Lai, *Adv. Funct. Mater.*, 2018, **28**, 1707415.
15 S. N. Zhang, J. Y. Huang, Y. X. Tang, S. H. Li, M. Z. Ge, Z. Chen, K. Q. Zhang and Y. K. Lai, *Small*, 2017, **13**, 1600687.
16 G. M. Gong, K. Gao, J. T. Wu, N. Sun, C. Zhou, Y. Zhao and L. Jiang, *J. Mater. Chem. A*, 2015, **3**, 713–718.
17 B. Su, Y. Tian and L. Jiang, *J. Am. Chem. Soc.*, 2016, **138**, 1727–1748.
18 L. Wang, C. L. Gao, Y. Hou, Y. Zheng and L. Jiang, *J. Mater. Chem. A*, 2016, **4**, 18289–18293.
19 N. Li, L. Wu, C. Yu, H. Dai, T. Wang, Z. C. Dong and L. Jiang, *Adv. Mater.*, 2018, **30**, 1703838.
20 Y. Rahmawan, L. B. Xu and S. Yang, *J. Mater. Chem. A*, 2013, **1**, 2955–2969.
21 C. R. Crick, J. C. Bear, A. Kafizas and I. P. Parkin, *Adv. Mater.*, 2012, **24**, 3505–3508.
22 S. Yu, Z. G. Guo and W. M. Liu, *Chem. Commun.*, 2015, **51**, 1775–1794.

This journal is © The Royal Society of Chemistry 2018

Open Access Article. Published on 23 August 2018. Downloaded on 3/29/2024 10:03:19 AM.
This article is licensed under a Creative Commons Attribution 3.0 Unported Licence.

23 L. B. Xu, R. G. Karunakaran, J. Guo and S. Yang, *ACS Appl. Mater. Interfaces*, 2012, **4**, 1118–1125.
24 C. R. Crick, J. A. Gibbins and I. P. Parkin, *J. Mater. Chem. A*, 2013, **1**, 5943–5948.
25 W. B. Zhang, Z. Shi, F. Zhang, X. Liu, J. Jin and L. Jiang, *Adv. Mater.*, 2013, **25**, 2071–2076.
26 M. Z. Ge, C. Y. Cao, J. Y. Huang, X. N. Zhang, Y. X. Tang, X. R. Zhou, K. Q. Zhang, Z. Chen and Y. K. Lai, *Nanoscale Horiz.*, 2018, **3**, 235–260.
27 S. Martin and B. Bhushan, *J. Colloid Interface Sci.*, 2017, **488**, 118–126.
28 F. Zhang, Z. W. Shi, Y. J. Jiang, C. Y. Xu, Z. H. Wu, Y. Y. Wang and C. S. Peng, *Appl. Surf. Sci.*, 2017, **407**, 526–531.
29 X. Deng, L. Mammen, Y. F. Zhao, P. Lellig, K. Mullen, C. Li, H. J. Butt and D. Vollmer, *Adv. Mater.*, 2011, **23**, 2962–2965.
30 Y. K. Lai, Y. X. Tang, J. J. Gong, D. G. Gong, L. F. Chi, C. J. Lin and Z. Chen, *J. Mater. Chem.*, 2012, **22**, 7420–7426.
31 H. Yoon, H. Kim, S. S. Latthe, M. W. Kim, S. Al-Deyab and S. S. Yoon, *J. Mater. Chem. A*, 2015, **3**, 11403–11410.
32 H. Y. Ji, G. Chen, J. Yang, J. Hu, H. J. Song and Y. T. Zhao, *Appl. Surf. Sci.*, 2013, **266**, 105–109.
33 J. T. Han, S. Y. Kim, J. S. Woo and G. W. Lee, *Adv. Mater.*, 2008, **20**, 3724–3727.
34 D. M. Chun, G. Davaasuren, C. V. Ngo, C. S. Kim, G. Y. Lee and S. H. Ahn, *CIRP Ann.*, 2014, **63**, 525–528.
35 G. Davaasuren, C. V. Ngo, H. S. Oh and D. M. Chun, *Appl. Surf. Sci.*, 2014, **314**, 530–536.
36 W. H. Huang and C. S. Lin, *Appl. Surf. Sci.*, 2014, **305**, 702–709.
37 I. U. Vakarelski, N. A. Patankar, J. O. Marston, D. Y. Chan and S. T. Thoroddsen, *Nature*, 2012, **489**, 274–277.
38 F. Li, M. Du, Z. Zheng, Y. H. Song and Q. Zheng, *Adv. Mater. Interfaces*, 2015, **2**, 1500201.
39 N. J. Shirtcliffe, G. McHale and M. I. Newton, *J. Polym. Sci., Part B: Polym. Phys.*, 2011, **49**, 1203–1217.
40 M. J. Powell, D. B. Potter, R. L. Wilson, J. A. Darr, I. P. Parkin and C. J. Carmalt, *Mater. Des.*, 2017, **129**, 116–124.
41 C. R. Crick and I. P. Parkin, *Chem. Commun.*, 2011, **47**, 12059–12061.
42 C. Kapridaki, A. Verganelaki, P. Dimitriadou and P. Maravelaki-Kalaitzaki, *Materials*, 2018, **11**, 684.
43 L. Tellez, J. Rubio, F. Rubio, E. Morales and J. L. Oteo, *J. Mater. Sci.*, 2003, **38**, 1773–1780.
44 C. Kapridaki and P. Maravelaki-Kalaitzaki, *Prog. Org. Coat.*, 2013, **76**, 400–410.
45 Y. Li, B. P. Zhang, C. H. Zhao and J. X. Zhao, *J. Mater. Res.*, 2012, **27**, 3141–3146.
46 S. S. Latthe, H. Imai, V. Ganesan and A. V. Rao, *Appl. Surf. Sci.*, 2009, **256**, 217–222.
47 F. Gherardi, S. Goidanich, V. Dal Santo and L. Toniolo, *Angew. Chem., Int. Ed.*, 2018, **57**, 7360–7363.
48 C. Kapridaki, L. Pinho, M. J. Mosquera and P. Maravelaki-Kalaitzaki, *Appl. Catal., B*, 2014, **156–157**, 416–427.
49 S. Rasalingam, H. S. Kibombo, C.-M. Wu, S. Budhi, R. Peng, J. Baltrusaitis and R. T. Koodali, *Catal. Commun.*, 2013, **31**, 66–70.
50 A. Y. Zhuang, R. J. Liao, Y. Lu, S. C. Dixon, A. Jiamprasertboon, F. Z. Chen, S. Sathasivam, I. P. Parkin and C. J. Carmalt, *ACS Appl. Mater. Interfaces*, 2017, **7**, 42327–42335.
51 S. H. Li, J. Y. Huang, M. Z. Ge, C. Y. Cao, S. Deng, S. N. Zhang, G. Q. Chen, K. Q. Zhang, S. S. Al-Deyab and Y. K. Lai, *Adv. Mater. Interfaces*, 2015, **2**, 1500220.
52 J. Y. Huang, S. H. Li, M. Z. Ge, L. N. Wang, T. L. Xing, G. Q. Chen, X. F. Liu, S. S. Al-Deyab, K. Q. Zhang, T. Chen and Y. K. Lai, *J. Mater. Chem. A*, 2015, **3**, 2825–2832.